

Dual-Layer Dual-Patch EBG Structure for Isolation Enhancement and Correlation Reduction in MIMO Antenna Arrays

Oludayo Sokunbi and Hussein Attia*

Abstract—This paper proposes a novel electromagnetic band gap (EBG) structure based on a dual-layer dual-patch unit (DLDP-EBG) cell to improve isolation and decrease envelope correlation between MIMO slot antenna array elements. A wideband MIMO slot antenna array operating in the frequency range of 4.2–6.5 GHz (43%) is deployed. The antenna array is based on slotted rectangular microstrip radiating elements printed on the top surface of two stacked FR4 substrates to widen the array impedance bandwidth. A 2×7 dual-layer DLDP-EBG unit cell is inserted between the array elements to reduce the mutual coupling and deflect the individual beams of each antenna in opposite directions. An isolation improvement of up to 56 dB is maintained throughout the working bandwidth of the antenna, when the EBG is inserted. Also, the DLDP-EBG unit cells reduce the envelope correlation coefficient by 5–30 dB across the whole operating bandwidth by deflecting the radiation beams of the individual antenna elements in opposite directions. The MIMO array gain and radiation efficiency have been improved after using the EBG structure due to the reduction in mutual coupling and surface wave mitigation between the array elements. The proposed low-profile MIMO slot antenna array is the first in literature to exhibit such wideband isolation improvement, gain enhancement, and correlation reduction behavior simultaneously.

1. INTRODUCTION

MIMO antennas are increasingly employed in modern wireless systems to enhance the system's capacity without necessarily increasing the bandwidth and transmitted power in a multipath environment [1]. The key factors that determine the overall communication effectiveness of a MIMO antenna in a MIMO system is the antenna channel environment and antenna properties [2]. Envelope correlation coefficient (ECC) is a characteristic parameter that considers these two factors. The ECC can be calculated in terms of far-field properties or S -parameters [3]. The ECC calculated in terms of S -parameters considers S_{21} between the individual antennas making up the MIMO array system. It is easy and fast to calculate but is unreliable as it assumes that the antenna efficiency is 100%, which is not practicable. On the other hand, mutual coupling reduction (i.e., reduced S_{21}) is usually based on port isolation [4].

Electromagnetic Band Gap (EBG) structures have been greatly employed in antenna structures because of their ability to inherently mitigate the propagation of electromagnetic waves over a certain bandgap. Hence, they are able to increase isolation by controlling space and surface waves in MIMO antenna arrays [5–7]. Microstrip technology suffers from pronounced surface waves due to higher substrate height and dielectric constant [8]. This makes mutual coupling a significant issue in microstrip MIMO antennas. EBG structures have been used to reduce mutual coupling and correlation between MIMO patch antenna array elements. Although mutual coupling reduction (measured through the transmission coefficient S_{21}) in MIMO antennas can be accompanied by correlation reduction, it is

Received 26 November 2019, Accepted 31 January 2020, Scheduled 31 March 2020

* Corresponding author: Hussein Attia (hattia@kfupm.edu.sa).

The authors are with the Electrical Engineering Department, King Fahd University of Petroleum and Minerals (KFUPM), Dhahran 31261, Saudi Arabia.

not necessarily a guarantee [9]. Other methods have therefore been proposed to strictly minimize the correlation between MIMO antennas [9–14]. These methods such as having a superstrate above the MIMO antennas may not decrease S_{21} between the antennas [3]. However, it will be a tremendous achievement in MIMO array design if both mutual coupling and ECC can be simultaneously reduced by beam deflection. Many publications have discussed different methods of increasing isolation in MIMO antennas with some accompanied correlation reduction. In [7], a 10 dB isolation improvement was recorded using slotted-complimentary split ring resonators (SRR). The authors in [15] used a stacked substrate to improve isolation by 6 dB. A 26.2 dB isolation improvement using a pair of parallel coupled line resonators at 3.5 GHz was recorded in [16]. Also, a 22 dB wideband (47%) mutual coupling reduction was achieved in [17] using wideband neutralization line and a metal strip, but the fabricated antenna had a high profile because of the vertical placement of the feeding cable to avoid the leaking currents getting excited over the ground plane. In [18], a 14 dB isolation improvement was recorded with a corresponding ECC reduction when using an array of complementary split-ring resonators (CSR) between slot antenna arrays. Isolation improvements of 27 dB and 40 dB, respectively, in the E - and H -planes have been achieved in [19] with low ECC. A dual layer short wire and an EW-shaped parasitic strip were used as isolation elements to achieve 25 dB isolation improvement with low ECC in [20]. In [21], the authors achieved isolation improvement in the 3.17–4.15 GHz frequency band using a fractal decoupling structure. The authors in [22] achieved 22.7 dB isolation improvement using a fractal EBG structure among four patch antennas. In [23], the authors used a dual-layer EBG structure to increase the operating bandwidth of a sabre-type antenna around 1.4 GHz to 24.4%. Elliptical split ring resonators were used in [24] to improve isolation by 19 dB over 5.1–5.9 GHz. A multilayer single unit cell EBG structure was used by the authors in [25] to accomplish a 28 dB isolation improvement. However, the overall profile of the antenna became enlarged because of the multilayer structure. In [26], a one-dimensional 10-layer EBG structure was used for noise suppression and impedance bandwidth enhancement for sub-6 GHz applications. Sixteen multilayer EBG unit cells for electromagnetic noise suppression were employed by the authors in [27] for multilayer printed circuit boards.

It is evident that most of the aforementioned work has concentrated on isolation improvement in antenna arrays over narrow bandwidths. This paper therefore presents a novel dual-layer dual-patch (DLDP) EBG structure that can improve the isolation between MIMO slot antenna array elements by 10–56 dB over the frequency range 4.2–6.5 GHz. This paper is the *first in literature* to use a multilayer EBG structure for both mutual coupling mitigation and ECC reduction by deflecting the main beams of the antenna in opposite directions. The paper is presented as follows. Section 2 demonstrates the DLDP-EBG unit cell design. Section 3 describes the integration of the DLDP-EBG unit cells and a slotted microstrip MIMO antenna array. Section 4 presents the measured results and compares them with the simulated results. Section 5 concludes the paper.

2. DUAL-LAYER DUAL-PATCH EBG (DLDP-EBG) UNIT CELL DESIGN

The DLDP-EBG unit cell used in this work exhibits periodic dimension $L_p \times W_p$ where $L_p = 13$ mm and $W_p = 5.032$ mm as shown in Fig. 1. It comprises a total of six EBG patches arranged vertically from top to bottom, and the ground. Moving upwards from the ground, first there are two EBG patches of unequal dimensions $L_1 \times W_p$ where $L_1 = 6$ mm, and a square-shaped EBG of dimensions $L_2 \times L_2$ where $L_2 = 4.6$ mm. The dimensions of the two unequal patches, as well as the diameter of the via are obtained using parametric analysis in CST microwave studio, and the optimum values are employed. The EBG patches are separated by $g = 0.125$ mm. Moving upwards, the third and fourth EBG patches and the fifth and sixth EBG patches are also separated by g . Two FR4 substrates each with a relative permittivity of 4.3, thickness of 1.6 mm, and loss tangent of 0.025 are used between the ground and the first two EBGs, as well as between third, fourth, and fifth, sixth EBGs. The EBG patches are located at $s = 1.1375$ mm away from the substrate edge on both sides. Four vias are used in this unit cell, each extending from top of all the six patches to bottom of each substrate, and are located at the centre of the patches. Each via has 0.6 mm and 0.78 mm as inner and outer diameters, respectively. A glue having the same material properties as the FR4 substrate but with thickness 0.02 mm is used in between the two substrates. This glue is used due to the fabrication requirement. The EBG patches and ground plane have been made to the same thickness of 0.035 mm.

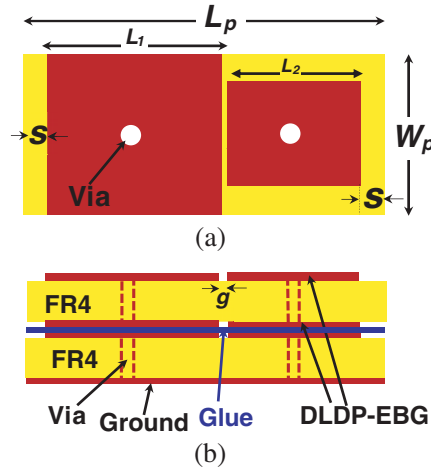


Figure 1. Dual-layer dual-patch EBG (DLDP-EBG) unit Cell: (a) Top view, and (b) side view.

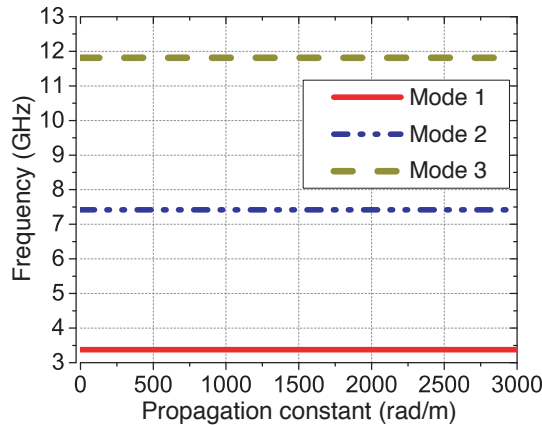


Figure 2. Dispersion diagram of the DLDP-EBG unit cell employed to create a wide stop band between 3.37–7.40 GHz.

The dispersion diagram of this DLDP-EBG unit cell is depicted in Fig. 2. It is clear from Fig. 2 that the bandgap is around 3.38–7.40 GHz between modes 1 and 2. This large rejection band is made possible by the combined multiple resonances created by the dual layers of EBG structures. The dispersion diagram of the proposed DLDP-EBG unit cell was calculated using the commercial EM software CST Eigenmode Solver, in which periodic boundary conditions are used on the four side walls of the unit-cell to mimic an infinite two-dimensional structure. The Eigenmode Solver calculates the electromagnetic fields, as well as the frequency bandwidth in the absence of any excitation. Over the frequency range of interest, the unit cell behaves as a high impedance surface, in order to inhibit the propagation of electromagnetic waves. It should be noted that the 3.38–7.40 GHz stopband illustrated by the dispersion diagram assumes that the unit cell is infinite. However, in reality, only a limited number of unit cells can be placed between the MIMO slot antenna array elements to reduce mutual coupling and ECC. Specifically, a finite two-dimensional array of 2×7 unit cells is used in this paper to reduce the mutual coupling and ECC over the frequency range of 4.2–6.5 GHz as illustrated in the next sections.

3. DLDP-EBG MIMO SLOT ARRAY ANTENNA

The whole MIMO slot antenna array measures $57.5 \text{ mm} \times 120.8 \text{ mm}$ as shown in Fig. 3. The slot antenna array consists of two printed patches on the top surface of two stacked FR4 substrates in order

to increase the impedance bandwidth of the antenna. Each printed patch has dimensions of $e \times c$, where $e = 33.54$ mm and $c = 34$ mm. A square slot of dimensions $d \times d$, where $d = 20$ mm, is etched on the two printed patches and rotated by 45° . A stub of dimensions $L = 7$ mm \times $W = 1.9$ mm is printed at a distance of 0.542 mm from one end of the slots in order to match the antenna [8]. The MIMO slot antenna is fed by an aperture-coupled stripline (indicated by black dotted line in Fig. 3), printed on the bottom substrate. The length of the stripline is 38 mm, and the width is 3.5 mm, with 0.035 mm thickness. The slots help to further increase the current paths (i.e., adding extra effective inductance) in the antenna which can increase the impedance bandwidth. Additionally, the slots also enable antenna miniaturisation for PCB technology while realising bigger bandwidth. The stubs are added to the slots in order to match the antenna over such a larger impedance bandwidth. The parameters of the stub are also optimized to obtain the best results. The length and width of the feeding strip line are also calculated using microstrip line equations in order to correctly

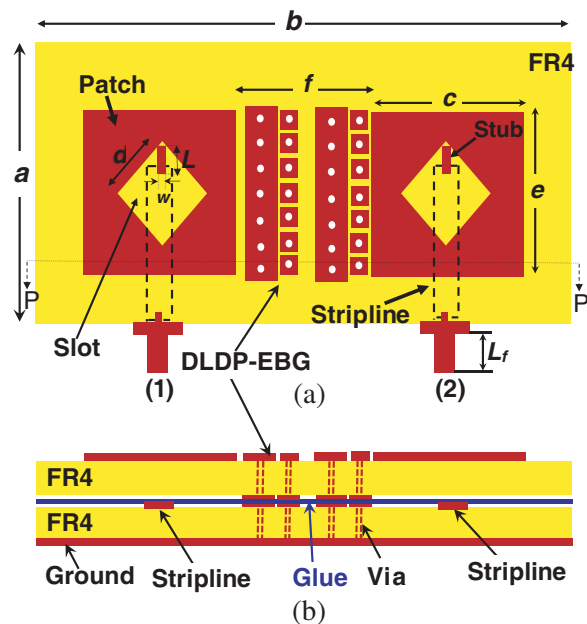


Figure 3. DLDP-EBG MIMO antenna. (a) Top view. (b) Cross section view along the dash line PP'.

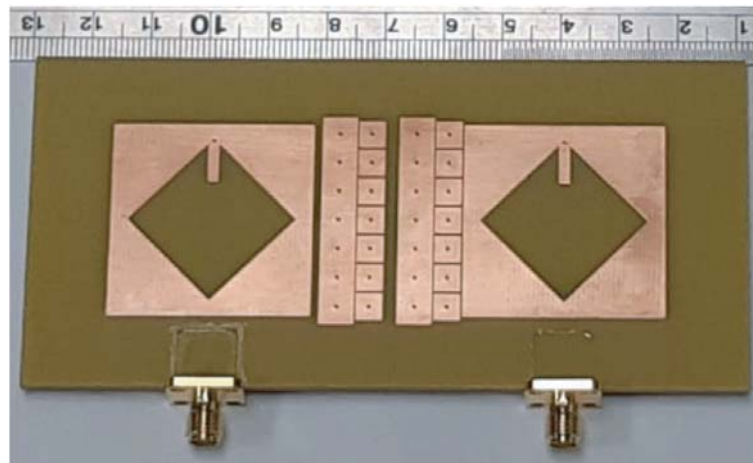


Figure 4. Top view of the Fabricated DLDP-EBG MIMO antenna.

match the impedance of the line to the antenna. The spacing between the two antennas is $f = 25.2$ mm ($0.42\lambda_0$) (λ_0 is the wavelength in free space at the centre frequency of 5 GHz).

The two substrates are separated by 0.09 mm, and a glue of thickness 0.02 mm, with the same dielectric constant as FR4 is used to stick the two substrates together as shown in Fig. 3. It should be noted that the via does not extend from the top patch to the ground. Instead, it extends only from the top to bottom of each substrate, just as presented in the unit cell. This is implemented in order to allow fabrication as discussed in the previous section. A 2×7 array of the DLDP unit cells is arranged between the two MIMO slot antennas. Fig. 4 shows the top view of the fabricated proposed antenna while Fig. 5 shows the measurement setup in an anechoic chamber where one antenna is fed, and the other is terminated by a 50-ohm matched load.



Figure 5. Radiation pattern measurement setup of the fabricated DLDP-EBG MIMO antenna.

4. ANALYSIS OF RESULTS

This section elaborates the measured and simulated results of the DLDP-EBG MIMO antenna. Fig. 6 depicts the simulated and measured S -parameter magnitudes of the DLDP-EBG MIMO antenna. The measured impedance bandwidth (i.e., S_{11}) covers the bandwidth 4.2–6.5 GHz. It is clear that the simulated and measured S -parameters of the antennas have a strong correlation. The slight discrepancy is linked to the difference in the electrical properties of the FR4 material used in simulation and fabrication. Also, it can be observed that S_{11} and S_{22} of the antenna are not exactly the same due to the unsymmetrical shape of the unit cell used in the DLDP-EBG structure that is composed of two unequal patches. Fig. 7 compares the simulated and measured isolations of the array only (i.e., the MIMO slot patch antenna array only without the DLDP-EBG unit cells between them) and the DLDP-EBG MIMO antenna. It is obvious that the coupling is reduced by 10–56 dB over the bandwidth of 4–7 GHz, with the highest reduction observed around 5.25 GHz. Also, the simulated and measured S_{21} magnitudes are closely matched. The disparity between the simulated and measured results in Fig. 7 is a result of the predicted differences between the practical electrical properties (permittivity, conductivity, and loss tangent) of the FR4 material employed in measurements and the standard values used in CST simulations by default. In fact, the sophisticated two-layer layout of the proposed antenna may be misaligned in the assembly process. This is because the fabrication requirements allow the use of glue with the same material properties as the substrate, but with a thickness of 0.02 mm, as shown in Fig. 1. This is required to enable through-hole plating. Hence, simulation results of 56 dB highest reduction at 5.25 GHz are accounted in this paper.

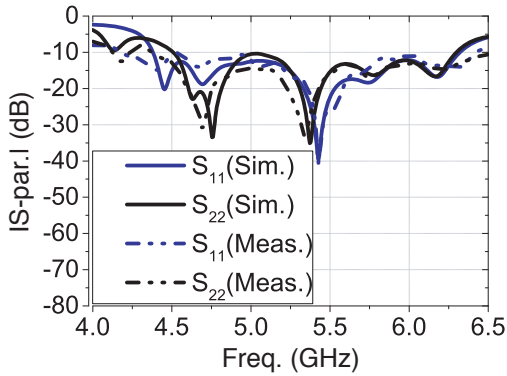


Figure 6. Simulated and measured S -parameter magnitudes of the DLDP-EBG MIMO antenna.

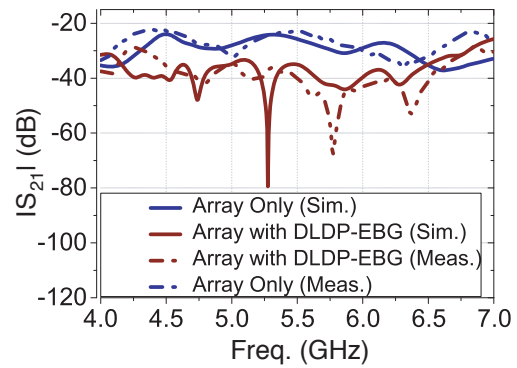


Figure 7. Comparison between S_{21} magnitudes of the array only and proposed DLDP-EBG MIMO antenna array.

Figure 8 shows the consequences of changing the number of DLDP-EBG unit cells on the isolation characteristics of the antenna. It is evident that the proposed DLDP-EBG array size of 2×7 exhibits the best isolation over the 4–7 GHz bandwidth. Choosing any array size of the EBG structure above or below this optimum value will clearly decrease the isolation bandwidth or reduce the isolation between the two antennas. Fig. 9 depicts the effect of changing L_1 , which is the size of the bigger patch of the unit cell as seen in Fig. 1. The best isolation over large bandwidth is observed to be that of the proposed structure (i.e., $L_1 = 6$ mm). Using any other length of the unit cell patch will clearly decrease the isolation bandwidth or increase the coupling between the two slot antennas. These results show the significant effect of the unit cell dimensions on the isolation bandwidth and size of the proposed MIMO slot antenna array.

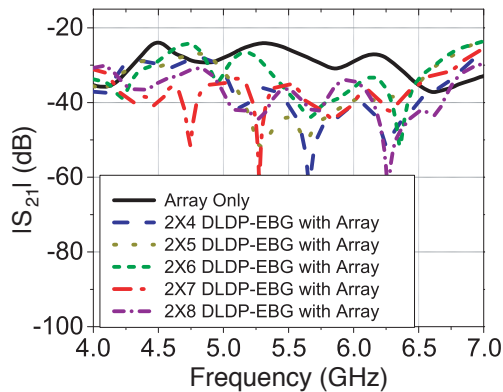


Figure 8. Effect of changing the number of DLDP-EBG unit cells on the isolation improvement of the proposed DLDP-EBG MIMO antenna.

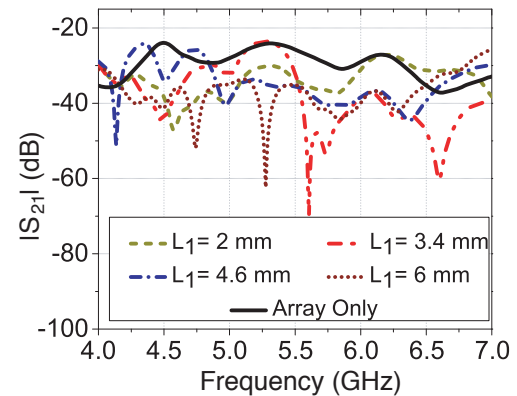


Figure 9. Effect of changing the size of the bigger patch of the unit cell size on the isolation improvement of the proposed DLDP-EBG MIMO antenna.

The impact of the DLDP-EBG unit cells on isolation enhancement is further analyzed by studying the current distribution on the surface of the array only (with no DLDP-EBG unit cells) compared with the proposed structure at 5.25 GHz. As evident in Fig. 10, the DLDP-EBG unit cells have absorbed most of the current travelling from antenna 1 to antenna 2 when port 1 is excited and port 2 terminated by a matched load. The current absorption is possible because the DLDP-EBG unit cells act as a high impedance surface at this frequency range. The same scenario will be observed if port 2 is excited and port 1 terminated by a matched load.

Figure 11 depicts the simulated and measured radiation patterns of the proposed DLDP-EBG

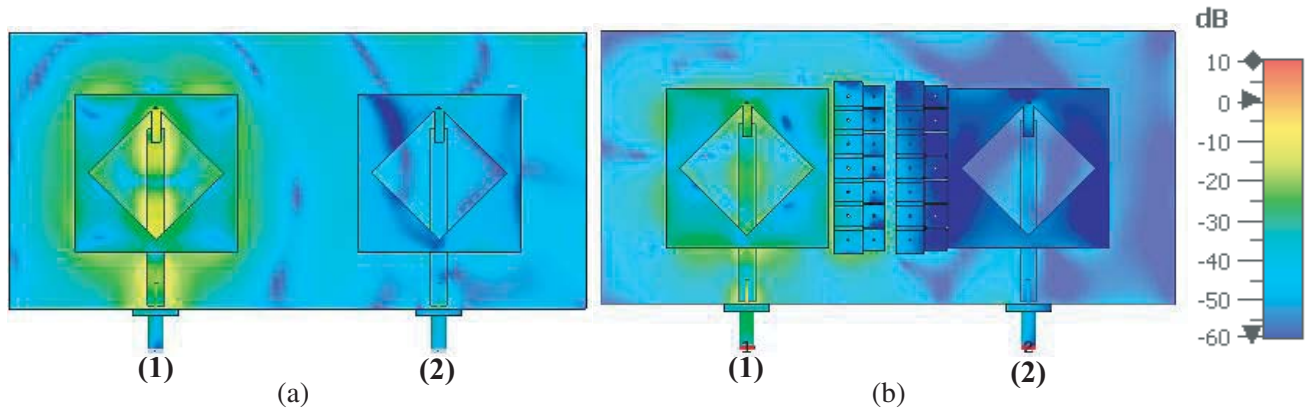
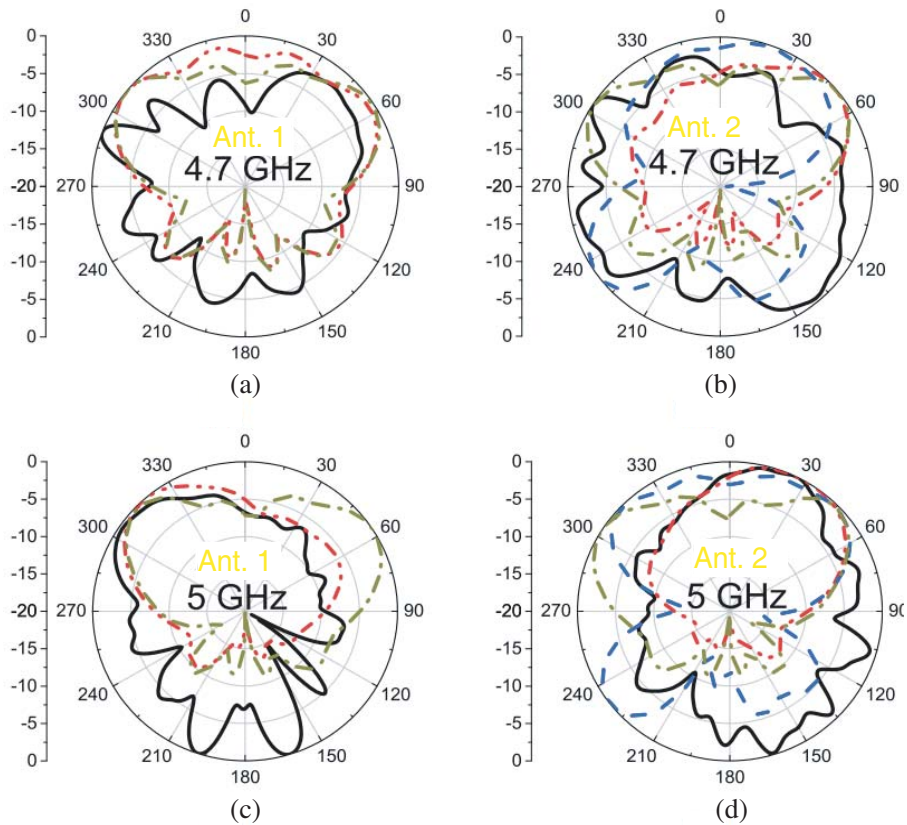


Figure 10. Surface current distribution at 5.25 GHz: (a) Array only, and (b) DLDP-EBG MIMO antenna.

MIMO antenna and antenna array only (without DLDP-EBG unit cells) at 4.7, 5, 5.2, and 6.4 GHz. The patterns have been measured with Microwave Vision Group (MVG), France [28]. The beams of the two antennas are observed to deflect in different directions with the addition of the DLDP-EBG unit cells at 5, 5.2, and 6.4 GHz. Consequently, the correlation between the two MIMO antennas is decreased as a result of the far-field interference reduction. This property demonstrates the usefulness and uniqueness of the proposed antenna, because the DLDP-EBG unit cells are able to simultaneously deflect the beams, as well as reduce coupling over a relatively large bandwidth.

However, beam deflection is not conspicuous at 4.7 GHz. Also, a closer look at Fig. 5 shows the blue cable used to feed antenna 2 while measuring the patterns. This cable exhibits high loss, leading to spurious radiation, hence, the increase in the backlobes of the measured radiation patterns as seen in Fig. 11. To verify this claim, the length of the coaxial feed of antenna 2 is increased by $L_f = 8$ mm



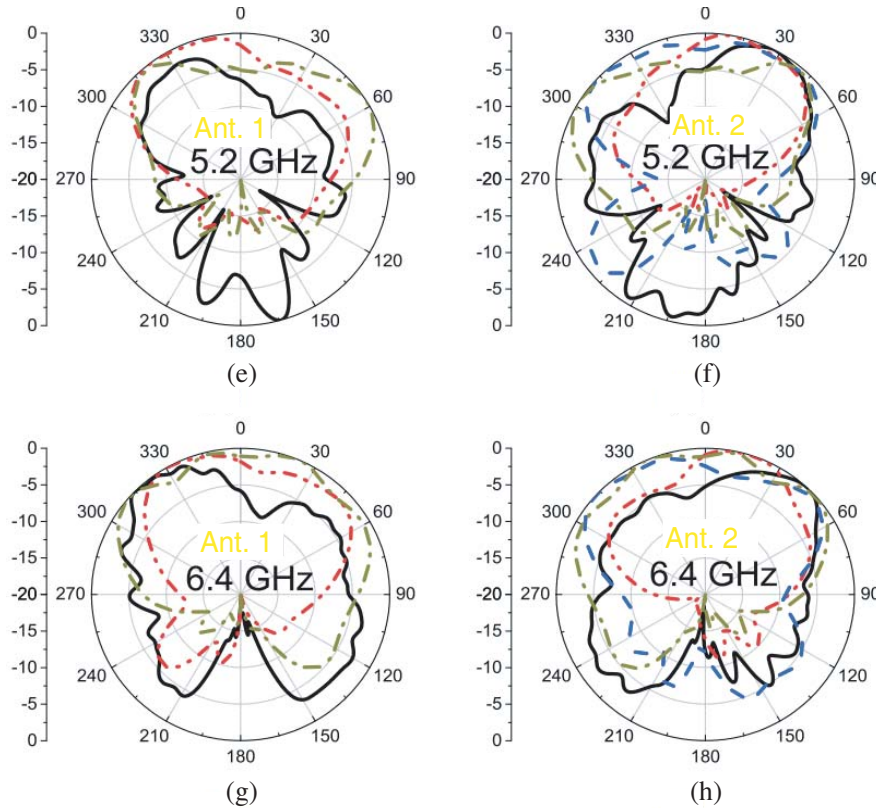


Figure 11. Radiation patterns of the DLDP-EBG MIMO antenna compared with the array only; the first and second columns of the figure are the patterns of antenna 1 and antenna 2, respectively. (— Measured DLDP-EBG MIMO antenna (Extended feed), - - - Simulated DLDP-EBG MIMO antenna (short feed), ··· Simulated DLDP-EBG MIMO antenna (Extended feed), - - - Simulated array-only (short feed)). (Extended feed: additional 8 mm feedline length, Short feed: normal SMA connector length).

(see Fig. 3) in CST simulations to almost match the length of the blue cable used for measurement. This results into increasing the simulated backlobes as seen by the blue dotted curves in Fig. 11. These updated results almost match the measured backlobes. On the other hand, the simulated patterns in the upper hemisphere agree considerably with the measured results.

To establish the leverage of the presented DLDP-EBG MIMO antenna over the conventional array only (with neither slot nor stub inserted in its elements), the slotted patch elements in Fig. 3 are replaced with the conventional patch as shown in Fig. 12. As depicted from Fig. 13, the achieved impedance bandwidth is just 2.6% (5.75–5.9 GHz) compared to 43% (4.2–6.5 GHz) of our proposed DLDP-EBG MIMO design. Also, the maximum isolation enhancement that can be achieved when the DLDP-EBG unit cells are inserted between the elements of the conventional patch array is about 10 dB within the 5.6–6.1 GHz bandwidth, compared to our proposed DLDP-EBG MIMO array that achieves 56 dB maximum isolation enhancement within 4–7 dB isolation bandwidth.

Figure 14 shows that the insertion of the DLDP-EBG unit cells increases the gain of the slotted antenna array by about 2 dB over that of the array only. This improvement is largely attributed to surface wave suppression between the two slot DLDP-EBG MIMO antennas. The two antennas can send and receive signals independently with less disruptions. It can also be observed that the measured gain is about 1 dB higher than the simulated gain mainly due to the alignment process, as well as the difference in the electrical properties of the FR4 material used in simulations and measurements as explained in the previous section. Also, Fig. 15 depicts a slight improvement in the total efficiency at 5 GHz when the DLDP-EBG MIMO antenna is compared to the array only, and this is due to the

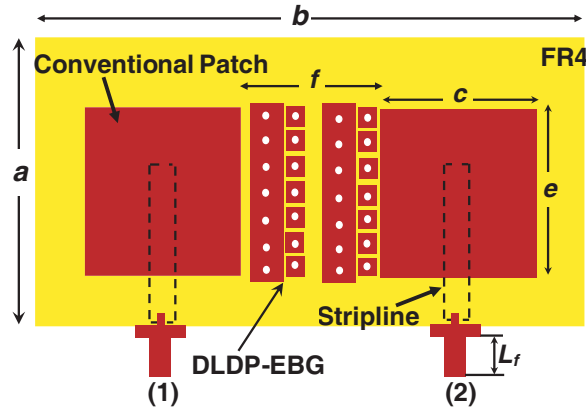


Figure 12. Conventional array only (with neither slot nor stub inserted in its elements) integrated with DLDP-EBG unit cells.

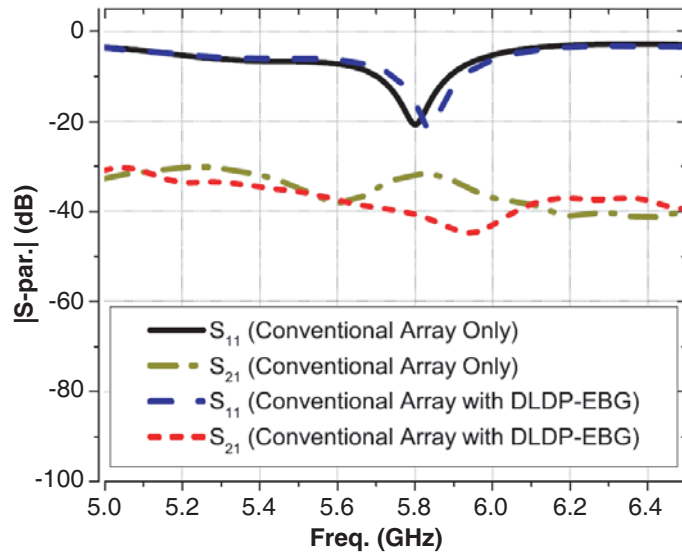


Figure 13. Comparison between the simulated S -parameter magnitudes of the conventional array only (with neither slot, stub, nor DLDP-EBG unit cells between its elements) and the same array (with neither slot nor stub inserted in its elements) with DLDP-EBG unit cells.

increased gain and surface wave mitigation between the two antennas. The overall efficiency is low because of the high-loss and inexpensive dual-layer FR4 substrate material used. The FR4 material is used as a proof-of-concept. In order to achieve better efficiency, a low-loss Rogers material can be considered.

Envelope correlation coefficient (ECC) is one of the essential performance metrics of a MIMO antenna. ECC gives an indication about how independent (i.e., less correlated) the radiation patterns of MIMO antennas are. A Lower ECC value indicates that the radiation patterns of the two antennas do not overlap, and hence, the adjacent MIMO antennas can send and receive independent data packages simultaneously. Moreover, less correlated MIMO antenna systems result in an enhanced data rate without the need for additional bandwidth or transmitted power. The ECC can be measured using port isolation, which is based on S -parameters. This method, however, is acceptable when the efficiency of the antenna is assumed to be ideal [2]. ECC based on S -parameters can be expressed as [29]:

$$ECC = \frac{|S_{11}^* S_{12} + S_{21}^* S_{22}|^2}{|(1 - |S_{11}^2| - |S_{21}^2|)(1 - |S_{12}^2| - |S_{22}^2|)|} \quad (1)$$

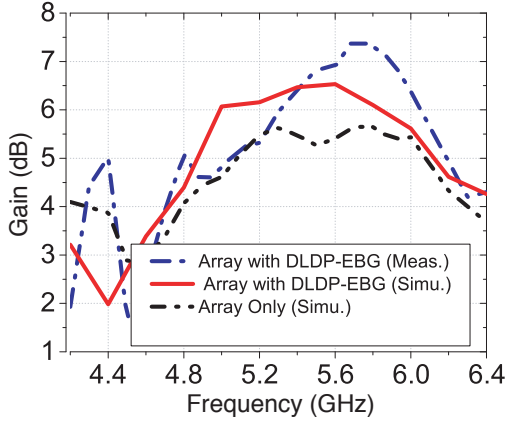


Figure 14. Measured and simulated gain of the DLDP-EBG MIMO antenna and the array only.

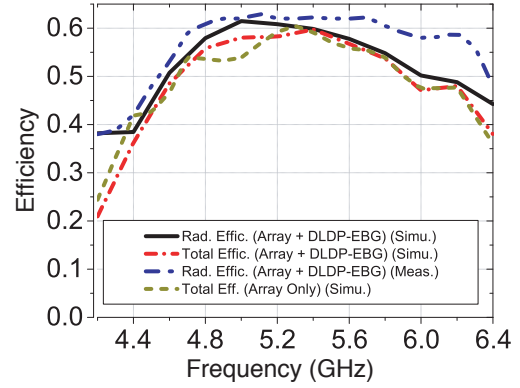


Figure 15. Measured and simulated efficiency of the DLDP-EBG MIMO antenna and the array only.

Figure 16 reveals the ECC of the two antennas using S -parameters. It is evident from Fig. 16 that there is correlation reduction about 10–35 dB across the entire bandwidth of the proposed DLDP-EBG MIMO antenna. Another method for calculating the correlation between two MIMO antennas is using the radiation pattern given by [29]:

$$ECC = \frac{|\iint_{4\pi} [A_1(\theta, \phi) \times A_2(\theta, \phi)] d\Omega|^2}{\iint_{4\pi} |A_1(\theta, \phi)|^2 d\Omega \iint_{4\pi} |A_2(\theta, \phi)|^2 d\Omega} \quad (2)$$

where $A_1(\theta, \phi)$ is the field pattern when antenna 1 is fed and antenna 2 terminated by a $50\ \Omega$ load. Calculation of ECC using the radiation pattern is more efficient because it considers the far-fields of the two antennas and is more reliable for lossy antennas [29]. Fig. 17 shows the ECC of the antennas using 3D radiation pattern. After placing the DLDP-EBG unit cells between the antennas, ECC is reduced by about 5–22 dB across the entire bandwidth.

It is widely believed that the reason for the high value of ECC around 4.7 GHz, as seen in Fig. 17, is that there is no beam tilting from both antennas at this frequency, as shown in the radiation patterns of Fig. 11. On the other hand, from Fig. 16 that shows the ECC calculated based on the results of S -par, it is evident that there is a substantial reduction in the ECC value of Fig. 16 around 4.7 GHz.

From Figs. 16 and 17, it can be observed that isolation between the two antennas is considerably

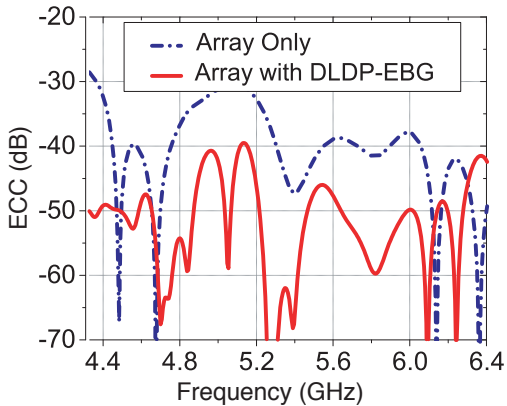


Figure 16. ECC of the array only and DLDP-EBG MIMO antenna based on S -parameters values.

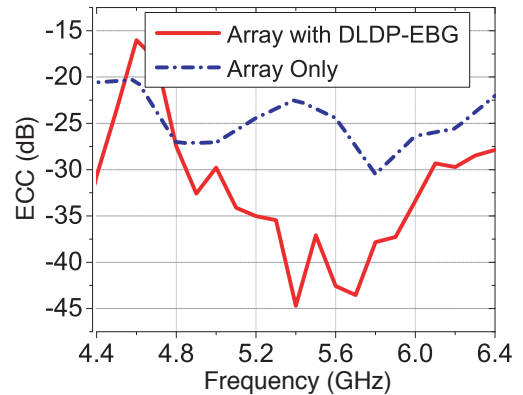


Figure 17. ECC of the array only and DLDP-EBG MIMO antenna based on the far-fields properties.

better before inserting the EBG structure. However, MIMO two-way (i.e., full-duplex) wireless communication systems and asynchronous two-way links (advantageous in networking applications) ideally require no mutual coupling between adjacent antennas in order to ensure concurrent data transmission and reception over the entire frequency band. Hence, S_{21} of such systems is required to be between -40 and -70 dB as illustrated in [30–32]. Therefore, the proposed DLDP-EBG MIMO antenna can be employed in such systems.

Table 1 shows a detailed comparison between the latest work in this area and the proposed design. It is evident that this work substantially outperforms previous work, especially in isolation improvement and S_{21} isolation bandwidth. Some of the cited work in the table shows lower edge-to-edge separation. They, however, do not show high impedance and isolation bandwidths compared to our work. Besides, this work also exhibits beam tilting and lower ECC based on far-fields; these achieved enhancements are clearly absent in most of the previous literature.

Table 1. Proposed design compared with recent literature.

Year/Ref.	S_{11} BW (%)	S_{21} BW (%)	Isolation improvement	Edge to Edge separation
2019 [19]	2	22	27–40 dB	$0.35\lambda_0$
2019 [20]	16	40	25 dB	$0.27\lambda_0$
2018 [22]	14.5	14.5	22.7 dB	$0.5\lambda_0$
2014 [33]	5	9.7	12 dB	$0.54\lambda_0$
2017 [34]	11.6	10	30 dB	$0.50\lambda_0$
Proposed	43	55	10–56 dB	$0.42\lambda_0$

5. CONCLUSION

A novel dual-Layer dual-patch EBG (DLDP-EBG) structure is introduced in this paper to considerably enhance the isolation between wideband MIMO antenna arrays. The DLDP-EBG structure is capable of increasing the isolation between closely spaced microstrip slot antennas by 10–56 dB over the entire bandwidth of 4.2–6.5 GHz. The DLDP structure is also able to decrease the correlation between the two antennas by deflecting the main radiation beams over the operating bandwidth of the antennas. Results from CST simulations and experiments demonstrate close coherence. The effects of changing the number of EBG unit-cells and the size of the unit-cell are also analyzed, and the most effective results are presented. Due to the enhanced port isolation and deflected beams of the antenna elements, the array gain and radiation efficiency have been improved after employing the DLDP-EBG structure. A detailed comparison with recent published work has been performed to show the uniqueness and usefulness of the proposed antenna. It is worth mentioning that the proposed MIMO radiating system integrated with an EBG metamaterial structure is the *first in literature* to exhibit such large isolation over wide bandwidth with beam deflections and gain enhancement.

ACKNOWLEDGMENT

The authors acknowledge the financial support from King Fahd University of Petroleum and Minerals (KFUPM), Saudi Arabia through DSR project No. SB181027.

REFERENCES

1. Foschini, G. J., “Layered space-time architecture for wireless communication in a fading environment when using multi-element antennas,” *Bell Labs Technical Journal*, Vol. 1, No. 2, 41–59, Autumn 1996.

2. Jensen, M. A. and J. W. Wallace, "A review of antennas and propagation for mimo wireless communications," *IEEE Transactions on Antennas and Propagation*, Vol. 52, No. 11, 2810–2824, Nov. 2004.
3. Hassan, T., M. U. Khan, H. Attia, and M. S. Sharawi, "An fss based correlation reduction technique for MIMO antennas," *IEEE Transactions on Antennas and Propagation*, Vol. 66, No. 9, 4900–4905, Sep. 2018.
4. Nadeem, I. and D. Choi, "Study on mutual coupling reduction technique for mimo antennas," *IEEE Access*, Vol. 7, 563–586, 2019.
5. Gauthier, G. P., A. Courtauy, and G. M. Rebeiz, "Microstrip antennas on synthesized low dielectric-constant substrates," *IEEE Transactions on Antennas and Propagation*, Vol. 45, No. 8, 1310–1314, Aug. 1997.
6. Sokunbi, O., H. Attia, and S. I. Sheikh, "Microstrip antenna array with reduced mutual coupling using slotted-ring ebg structure for 5g applications," *2019 IEEE International Symposium on Antennas and Propagation and USNC-URSI Radio Science Meeting*, 1185–1186, Jul. 2019.
7. Bait-Suwailam, M. M., O. F. Siddiqui, and O. M. Ramahi, "Mutual coupling reduction between microstrip patch antennas using slotted-complementary split-ring resonators," *IEEE Antennas and Wireless Propagation Letters*, Vol. 9, 876–878, 2010.
8. Sarin, V. P., N. Nassar, V. Deepu, C. K. Aanandan, P. Mohanan, and K. Vasudevan, "Wideband printed microstrip antenna for wireless communications," *IEEE Antennas and Wireless Propagation Letters*, Vol. 8, 779–781, 2009.
9. Sharawi, M. S., "Current misuses and future prospects for printed multiple-input, multiple-output antenna systems [wireless corner]," *IEEE Antennas and Propagation Magazine*, Vol. 59, No. 2, 162–170, Apr. 2017.
10. Li, M., B. G. Zhong, and S. W. Cheung, "Isolation enhancement for mimo patch antennas using near-field resonators as coupling-mode transducers," *IEEE Transactions on Antennas and Propagation*, Vol. 67, No. 2, 755–764, Feb. 2019.
11. Zhu, Y., Y. Chen, and S. Yang, "Decoupling and low-profile design of dual-band dual-polarized base station antennas using frequency-selective surface," *IEEE Transactions on Antennas and Propagation*, Vol. 67, No. 8, 5272–5281, Aug. 2019.
12. Li, M., L. Jiang, and K. L. Yeung, "Novel and efficient parasitic decoupling network for closely coupled antennas," *IEEE Transactions on Antennas and Propagation*, Vol. 67, No. 6, 3574–3585, Jun. 2019.
13. Sokunbi, O. and H. Attia, "Highly reduced mutual coupling between wideband patch antenna array using multiresonance EBG structure and defective ground surface," *Microwave and Optical Technology Letter*, 1–10, 2019.
14. Roshna, T. K., U. Deepak, V. R. Sajitha, K. Vasudevan, and P. Mohanan, "A compact uwb mimo antenna with re ctor to enhance isolation," *IEEE Transactions on Antennas and Propagation*, Vol. 63, No. 4, 1873–1877, Apr. 2015.
15. Rajo-Iglesias, E., O. Quevedo-Teruel, L. Inclan-Sainchez, and L.-E. Garcia-Munoz, "Design of a planar ebg structure to reduce mutual coupling in multilayer patch antennas," *2007 Loughborough Antennas and Propagation Conference*, Vol. 4, No. 4, 149–152, Apr. 2007.
16. Vishvakshan, K. S., K. Mithra, R. Kalaiarasan, and K. S. Raj, "Mutual coupling reduction in microstrip patch antenna arrays using parallel coupled-line resonators," *IEEE Antennas and Wireless Propagation Letters*, Vol. 16, 2146–2149, 2017.
17. Zhang, S. and G. F. Pedersen, "Mutual coupling reduction for UWB MIMO antennas with a wideband neutralization line," *IEEE Antennas and Wireless Propagation Letters*, Vol. 15, 166–169, 2016.
18. Ghosh, J., D. Mitra, and S. Das, "Mutual coupling reduction of slot antenna array by controlling surface wave propagation," *IEEE Transactions on Antennas and Propagation*, Vol. 67, No. 2, 1352–1357, Feb. 2019.
19. Radhi, A. H., R. Nilavalan, Y. Wang, H. Al-Raweshidy, A. A. Eltokhy, and N. A. Aziz, "Mutual coupling reduction with a novel fractal electromagnetic bandgap structure," *IET Microwaves*,

- Antennas Propagation*, Vol. 13, No. 2, 134–141, 2019.
20. Liu, F., J. Guo, L. Zhao, X. Shen, and Y. Yin, “A meta-surface decoupling method for two linear polarized antenna array in sub-6 GHz base station applications,” *IEEE Access*, Vol. 7, 2759–2768, 2019.
 21. Li, X., G. Yang, and Y. Jin, “Isolation enhancement of wideband vehicular antenna array using fractal decoupling structure,” *IEEE Antennas and Wireless Propagation Letters*, Vol. 18, No. 9, 1799–1803, Sep. 2019.
 22. Alibakhshikenari, M., B. S. Virdee, C. H. See, R. Abd-Alhameed, A. Hussein Ali, F. Falcone, and E. Limiti, “Study on isolation improvement between closely-packed patch antenna arrays based on fractal metamaterial electromagnetic bandgap structures,” *IET Microwaves, Antennas Propagation*, Vol. 12, No. 14, 2241–2247, 2018.
 23. Yuan, T., H. H. Ouslimani, A. C. Priou, G. Lacotte, and G. Collignon, “Dual-layer ebg structures for low-profile “bent” monopole antennas,” *Progress In Electromagnetics Research B*, Vol. 47, 315–337, 2013.
 24. Hafezifard, R., M. Naser-Moghadasi, J. R. Mohassel, and R. A. Sadeghzadeh, “Mutual coupling reduction for two closely spaced meander line antennas using metamaterial substrate,” *IEEE Antennas and Wireless Propagation Letters*, Vol. 15, 40–43, 2016.
 25. Movahedinia, R., M. Niroo-jazi, M. Akbari, A. R. Sebak, and M. R. Chaharmir, “Improvement of transmit-receive array antenna isolation by employing multilayer EBG structure,” *2015 IEEE International Conference on Ubiquitous Wireless Broadband (ICUWB)*, 1–4, Oct. 2015.
 26. Shen, C., T. Wu, C. Chen, and D. Han, “Miniaturized and bandwidth-enhanced multilayer 1-D EBG structure for power noise suppression,” *2014 IEEE International Symposium on Electromagnetic Compatibility (EMC)*, 357–361, Aug. 2014.
 27. Kim, M. and S. Ahn, “A compact and multi-stack electromagnetic bandgap structure for gigahertz noise suppression in multilayer printed circuit boards,” *Applied Sciences*, Vol. 7, 804, Aug. 2017.
 28. Microwave vision group (mvg), [Online], Available: <https://www.mvg-world.com/en/products/fieldproductfamily/antenna-measurement-2/starlab>.
 29. Blanch, S., J. Romeu, and I. Corbella, “Exact representation of antenna system diversity performance from input parameter description,” *Electronics Letters*, Vol. 39, No. 9, 705–707, May 2003.
 30. Khandani, A. K., “Two-way (true full-duplex) wireless,” *2013 13th Canadian Workshop on Information Theory*, 33–38, Jun. 2013.
 31. Khandani, A. K., “Methods for spatial multiplexing of wireless two-way channels,” patent number: 7817641, Oct. 19, 2010.
 32. Jain, M., J. Choi, S. I. Sheikh, T. M. Kim, D. Bharadia, S. Seth, K. Srinivasan, P. Levis, S. Katti, and P. Sinha, “Practical, real-time, full duplex wireless,” *MobiCom '11 Proceedings of the 17th Annual International Conference on Mobile Computing and Networking*, 301–312, Sep. 2011.
 33. Ghosh, C. K., R. Hazra, A. Biswas, A. K. Bhattacharjee, and S. K. Parui, “Suppression of cross-polarization and mutual coupling between dual trace dual column coaxial microstrip array using dumbbell-shaped resonator,” *Microwave and Optical Technology Letters*, Vol. 56, No. 9, 2182–2186, 2014.
 34. Karimian, R., A. Kesavan, M. Nedil, and T. A. Denidni, “Low-mutual-coupling 60-GHz MIMO antenna system with frequency selective surface wall,” *IEEE Antennas and Wireless Propagation Letters*, Vol. 16, 373–376, 2017.